Vegetation fire spread database: 85 wood wool shaving experiments at laboratory scale

A. Marchand, S. Ferriere, A. Collin, Pascal Boulet, Z. Acem, F. Demeurie, Jean-Yves Morel

Proposition of communication in **Fire Safety Journal** [Version: July 22, 2019]

Vegetation fire spread database: 85 wood wool shaving experiments at laboratory scale

A. Marchand, S. Ferriere, A. Collin*, P. Boulet, Z. Acem, F. Demeurie and J–Y. Morel

LEMTA, Université de Lorraine, CNRS

2 Avenue de la Forêt de Haye - TSA 60604 - 54518 Vandœuvre-lès-Nancy cedex, France

KEY WORDS: vegetation fire, experimental, image processing, laboratory-scale, database

ABSTRACT

This paper presents results obtained on 85 vegetation fire propagations carried out at an indoor platform on burning tables, considering no wind and no slope conditions. The fuel used is wood wool and has been properly described from the size distributions to the thermal degradation properties. Several fuel bed configuration have been tested: with 2-meter-length, the fuel bed width has been varied between 25 cm and 3.5 m and the fuel bed load was in the range from 0.1 to 1 kg/m^2. Experiments were focused on the effect of fuel bed width and fuel bed load on fire spread. Experiments are post-processed using an image processing method based on a direct linear transformation algorithm to track ignition and extinction fire line positions over time. A first analysis of this database is presented to study the evolutions of the Rate Of Spread (ROS) and on the fire zone depth (e_f) as a function of fuel bed width and fuel bed load. This new free-access online database gathers all data and aims at validating or calibrating vegetation fire spread models at laboratory scale in a controlled environment.

*Correspondence to: anthony.collin@univ-lorraine.fr

1. INTRODUCTION

Modeling of vegetation fire spreads requires both experimental and theoretical studies for a better understanding of propagation mechanisms and for evaluating quality of model predictions. Today, the variety of models is wide [1–3]. All of these models need experimental data for their calibration and their validation. This is true for the simplest ones based on empirical relationships [4], the finest numerical tools based on Computational Fluid Dynamics [5–7], cellular automata [8], small world networks [9] or for data-assimilation [10] which cannot be developed without dedicated experimental databases.

Laboratory-scale experiments provide well-known conditions for model calibration. On the contrary, this may be hardly ascertained in large-scale terrain tests. Preparation of such experiments requires considerable efforts: characterization of vegetation, safety requirements and so on. The dependence on weather conditions penalizes the control of experiment and limiting thus reproducibility. Any wind perturbations or meteorological change make simulations more difficult to calibrate or validate. Moreover, the number of sensors restricts the spatial resolution. Nevertheless, we can cite some attempts [11–13] that provide valuable data for validation [14]. Indoor experiments allow a better control of conditions during test with limited variability in fuel load, slope or wind. They usually concern moderate spatial and time scales, being therefore easy to prepare and to repeat. They become academical situations better aimed at validating and calibrating models. The remaining difficulty is the up-scaling of laboratory tests. We can find in literature many experiments at laboratory scale for a diverse kind of vegetation [15–17] with particularly Weise *et al.* [18] who provided an online database containing experimental data of forest fuel bed fire spread experiments.

The LEMTA laboratory built an experimental platform named PROMETHEI with the main objective of providing a free-access online database of laboratory-scale vegetation fires. A fire spread experiment can be conducted with the possibility of varying fuel type, fuel load, slope (with inclined tables) or wind conditions (with an indoor wind tunnel). We present here first results obtained with monochromatic cameras. Data consists of the positions of ignition and extinction lines reconstructed from grayscale images.

In this paper, we present a synthesis of 85 fire tests carried out for characterized wood wool. These tests are divided into two series of experiments:

- horizontal propagation, no wind, constant load, line ignition, and different fuel bed widths;
- horizontal propagation, no wind, constant fuel bed width, line ignition and different vegetation loads.

In these configurations, easy to handle for calibration tests, data includes fire line positions as a function of time. All data are available in free-access on the laboratory website [19]. The following sections detail vegetation properties (density, thermal properties ...), experimental set-up and finally the database.

2. EXPERIMENTAL SET-UP

In this section, we present results of 85 vegetation fire spreads propagated on 3 m $\times$ 4 m non-insulated burning steel tables. We conducted two series of experiments. The first one focused on changing the bed width between 0.25 m and 3.5 m at a constant fuel load of 0.5 kg/m^2. The second one concerned a variation of the fuel load between 0.1 kg/m^2 to 1 kg/m^2 at a constant 2 m fuel bed width. The ignition is along the whole width at one extremity of the table.

2.1 Vegetation characteristics

In this study, only wood wool was used as fuel. The Adrene Company (www.adrene.com) produced this wood wool from European silver firs, free of chemical treatment and dried through a natural process over one year.

This kind of fuel (in terms of fuel nature and vegetation medium) has no equivalence in the nature. However, this type of fuel is easily accessible (easy to find on the market) and thus allow us to perform many experiments in similar conditions of fuel. Moreover, the main advantage is its physical properties: the moisture content remains quasi-constant over the seasons.

2.1.1 Geometry

Wood wool is a non-homogeneous medium composed of fibers of different sizes. Fibers of a wood wool sample were analyzed to define the distributions of length, width, and thickness (fibers are rather parallelepiped than cylindrical). Figure 1 presents the resulting features. 304 wood wool fibers were characterized by a total mass of 4.830 g. Width and thickness were measured with a caliper.

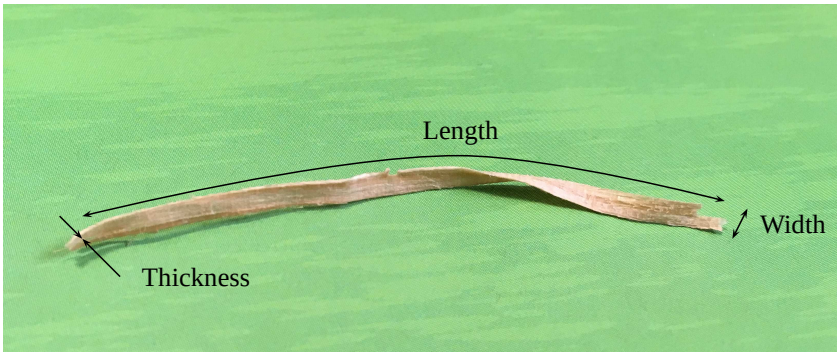

Figure 1 Definition of fiber dimensions

Feature	Length		Thickness		Width		Surface / Volume ratio	
Distribution law	Weibull		Normal		Normal		Normal	
Parameters	a [mm]	b [-]	μ [mm]	σ [mm]	μ [mm]	σ [mm]	μ [m^{-1}]	σ [m^{-1}]
Values	89.07	1.286	0.1632	0.056	1.9606	0.2198	14 617	4 657

Table 1 Parameters identified for the wood wool size distributions

Length The fiber length distribution is in a range of 4 mm to 316 mm. The mean value is about 82.4 mm with a standard deviation of 64.9 mm. In Figure 2(a), experimental results are given as a cumulative distribution function, noted here F. A Weibull law as the probability function, defined in Appendix section, shows a good agreement with experimental data with a maximal relative discrepancy about 8%. The probability density function, f, is also plotted in Figure 2(a) and parameters are reported in Table 1. It also shows that 80 % of the fiber lengths are smaller than 120 mm.

Thickness The thickness distribution provided by the measured wood wool fiber is plotted in Figure 2(b). The cumulative distribution function for the thickness presents more significant variations than the length distribution. Consequently, we consider a normal distribution, defined in Appendix section, to represent thickness distribution. Thicknesses vary between 0.05 mm and 0.58 mm, with a mean value μ = 0.1632 mm and a standard deviation σ = 0.056 mm. Figure 2(b) gathers the probability density function and the cumulative representation of the thickness. Results show a good agreement between numerical and experimental distributions with a maximum discrepancy of 10%.

Width The width distribution is plotted in Figure 2(c). Experimental results are in the range of 0.61 mm to 2.99 mm. The mean value is around 1.96 mm and the standard deviation is 0.22 mm. A normal law represents the fiber width distribution. Figure 2(c) shows that the identified normal law is relevant to represent the width distribution. The maximum relative discrepancies reaches 7%.

Surface-area-to-volume ratio Figure 2(d) shows the experimental particle surface-area-to-volume ratio and the numerical approximation using a normal distribution of the cumulative distribution. The mean value is about 14 600 m^{-1} and the standard deviation is close to 4 600 m^{-1}. These values are close to those given by Dickinson *et al.* [20] for Aspen wood excelsior estimated at about 13 200 m^{-1}. The maximal relative discrepancy between the experimental and the identified cumulative distribution reaches 15%.

2.1.2 Density

According to the supplier, the density may vary from 450 to 550 kg/m^3. As a verification test, the wood wool density was measured using a water displacement method. This approach consists in measuring the volume of an irregularly shaped object by immersing it in water. Measurements are achieved as fast as possible to avoid any variation in the moisture content of the sample of vegetation. Density is then deduced by:

$$\rho = \frac{m_{\text{fuel}}}{V_{\text{displaced}}} \tag{1}$$

where m_{fuel} is the sample weight and $V_{\text{displaced}}$ the variation volume of fluid after immersion. Measurements were repeated five times considering different weights of samples. The accuracy of the load cell is 0.0001 g (Δm). Using the logarithmic derivative approach, the relative error on the density estimation is given by:

$$\frac{\Delta\rho}{\rho} = \frac{\Delta m}{m_{\text{fuel}}} + 2\frac{\Delta V}{V_{\text{displaced}}} \tag{2}$$

The quality of density estimation is mostly controlled by the displaced fluid volume. This volume is equal to the difference between the volume after immersion (V_{after}) and the volume before immersion (V_{before}). For each volume, the accuracy of the measure is set at 5 mL. Consequently, the accuracy on the displaced fluid volume corresponds to 10 mL, or $2\Delta V$.

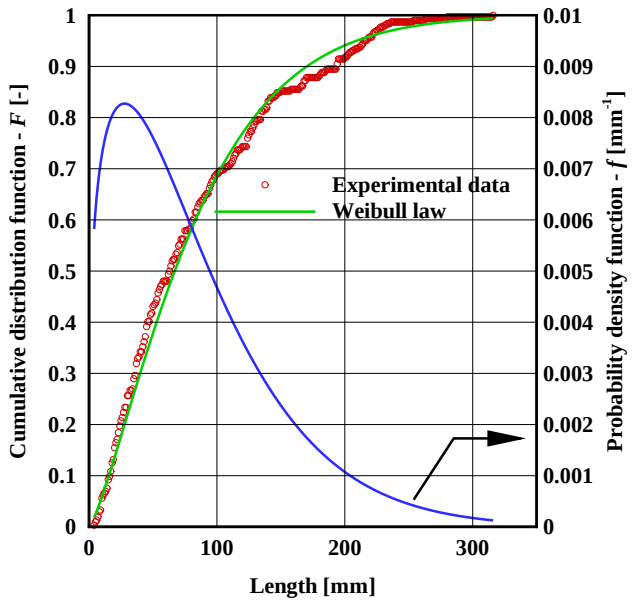

(a) Length

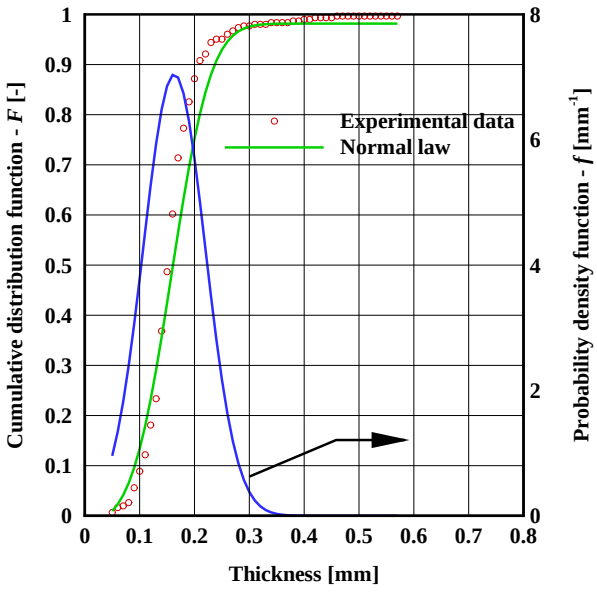

(b) Thickness

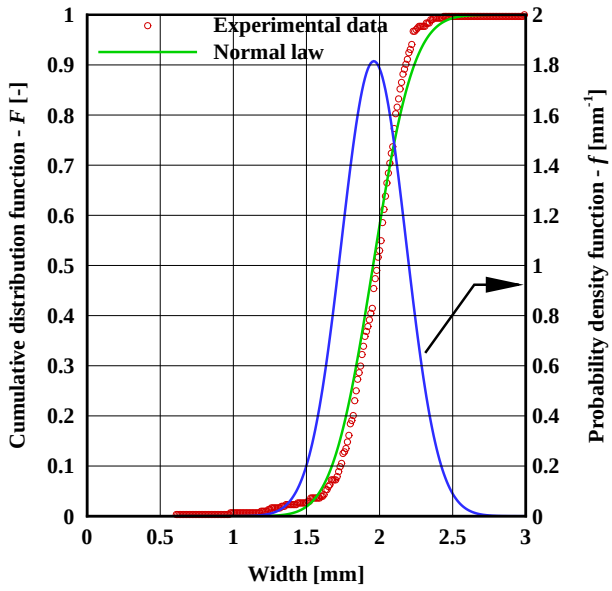

(c) Width

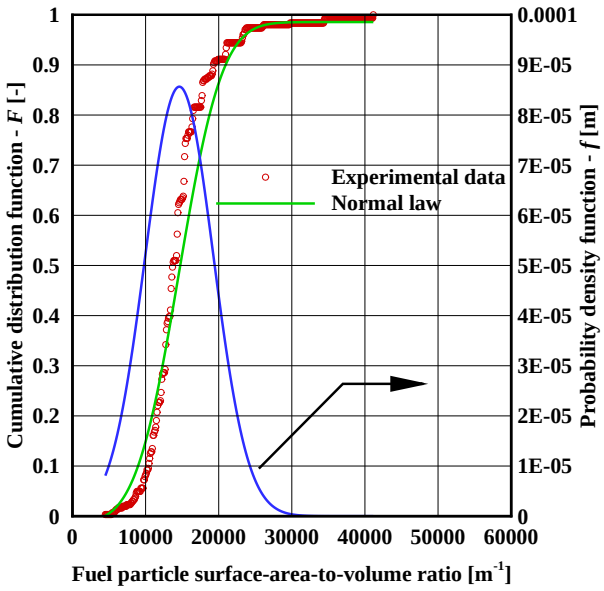

(d) Particle surface-area-to-volume ratio

Figure 2 Geometry distributions of the wood wool

Test	#1	#2	#3	#4	#5
Sample weight [g]	29.6125	30.5124	26.1437	30.1549	30.3278
Volume of the displaced fluid [mL]	[55 - 60]	[55 - 60]	[50 - 55]	[55 - 60]	[55 - 60]
Density [kg/m^3]	515	531	498	524	527
Confidence interval [kg/m^3]	[470 - 560]	[484 - 576]	[451 - 545]	[478 - 569]	[481 - 572]

Table 2 Experiments to determine the wood wool density

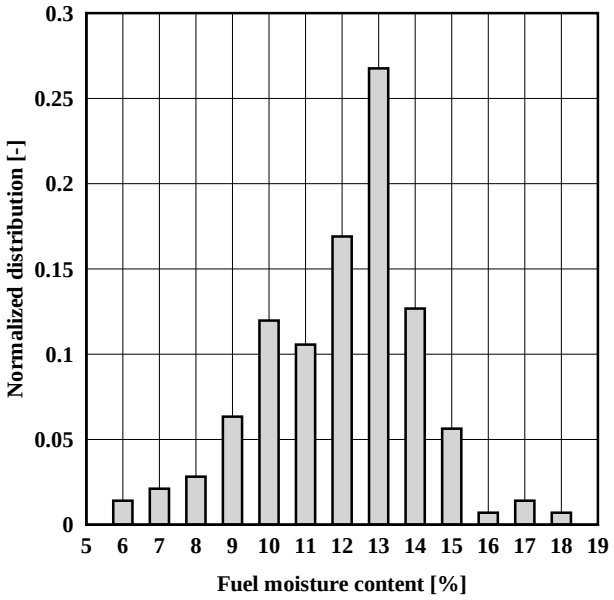

Figure 3 Distribution of the wood wool moisture content

Table 2 gathers the different results. The density varies between 515 to 531 kg/m^3. Nevertheless, absolute error observed for each test is large, close to 100 kg/m^3. The mean value is 519 kg/m^3.

2.1.3 Fuel moisture content

For this study, a PCE-MB 210C from PCE Instrument® was used to measure the wood wool moisture content. The moisture analyser can be used to heat a sample up to 160°C. A lower temperature at 110°C is used to avoid any matter transformation into pyrolysis gases. The sample can be dried at this constant temperature and it allows a quickest drying

rate without damaging the sample itself. The mass lost is measured during time and the drying process is stopped when the mass does not change for 10 seconds.

The moisture content can be calculated upon the basis of various mathematic formulas. For this study, we choose a moisture content (noted here w) defined as,

$$w = \frac{m_0 - m}{m_0} \tag{3}$$

where m_0 and m are respectively the initial mass of the sample and the final mass after the drying process. For each test, the initial mass was close to 160 mg.

A histogram presented in Figure 3 gathers 190 measurements (2 tests for each fire propagation). We observe that fuel moisture content varies between 5 and 18 %, which is not surprising owing to the various meteorological conditions observed during the test campaign. The first quartile is 10.4 % and the third quartile is 13.3 %. For each fire spread, the mean moisture content is measured and reported for each file of the database.

In this work, we did not consider the dry bases (mass of dry fuel per meter square) but for each test, the fuel moisture content was measured from a sample randomly extracted from fuel bed. Thus, the dry bases can be recovered.

2.1.4 Chemical composition

Thermogravimetric analysis (TGA) apparatus was used to measure the thermal degradation process of the wood wool in air condition. Figure 4(a) presents the normalized mass $\left(m^*(t) = \frac{m(t) - m(0)}{m(0)}\right)$ as a function of sample temperature for different temperature rates: 5, 10 and 20°C/min. All these tests started with an initial mass of 10 mg of wood wool. Figure 4(a) shows the wood composition:

- moisture, 6 - 7% of the total mass (depending on storage conditions);
- pyrolysis gases, 61% of the total mass;
- chars, 31% of the total mass;
- ashes, lesser than 1% of the total mass, mainly composed of mineral residues. The ash fraction (τ_r or ratio of residual mass) was estimated at 0.0027 gr of mineral/gr of dried wood.

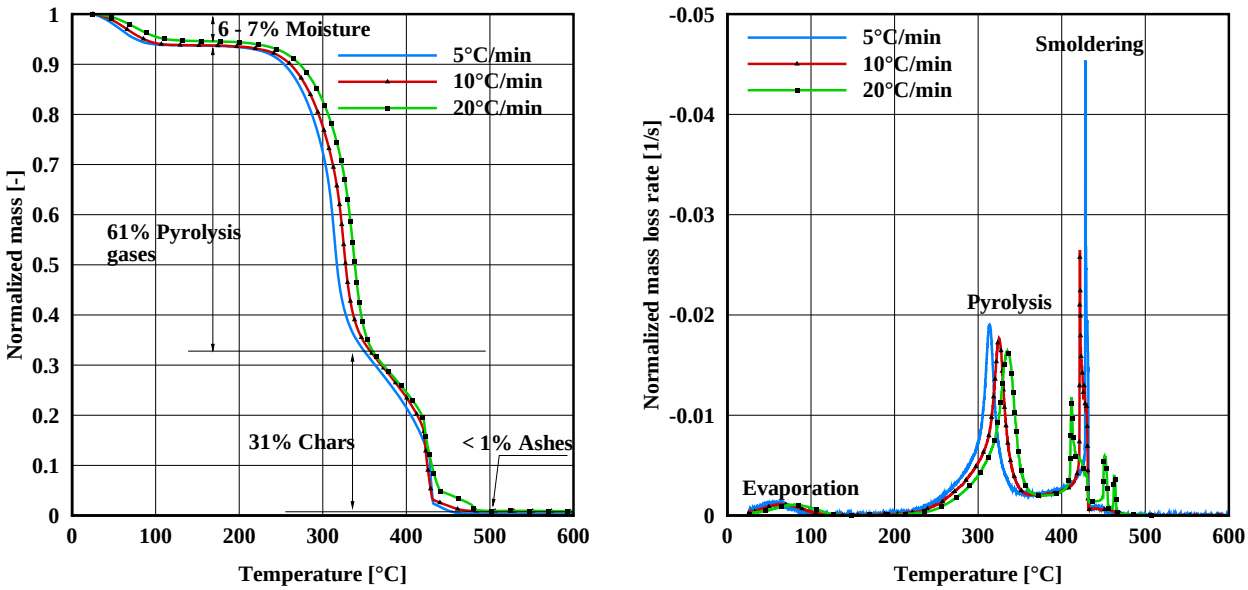

(a) Normalized mass obtained by thermogravimetric analysis versus the sample temperature

(b) Normalized mass loss rate versus the sample temperature

Figure 4 Thermal degradation features of the wood wool

Based on the normalized mass results, Mass loss rate (MLR) curves are then computed using 4th order-derivative approximations and are plotted in Figure 4(b). The thermal degradation of wood wool involves three steps:

(i) evaporation of moisture from vegetation between 50°C and 100°C.

(ii) generation of pyrolysis gases between 200 and 350°C due to thermal degradation of hemicellulose, cellulose, and lignin contained in wood. These results are common for organic materials as recalled by Di Blasi [21] for example. This step leads to a flaming combustion. Table 3 gives the maximal values reached by MLR as a function of temperature rates and the associated temperature peaks. These values change slowly with temperature rates.

(iii) oxidation of remaining chars beyond 350°C. This stage corresponds to a smouldering combustion.

2.1.5 Thermal properties

Supplementary physical properties were determined through dedicated experiments such as DSC and bomb calorimeter:

Temperature rates [°C/min]	5	10	20
Maximal values of the MLR [1/s]	-0.019	-0.0175	-0.0165
Temperature peak [°C]	313	324	335

Table 3 Maximal values of MLR and temperature peaks as a function of the temperature rates

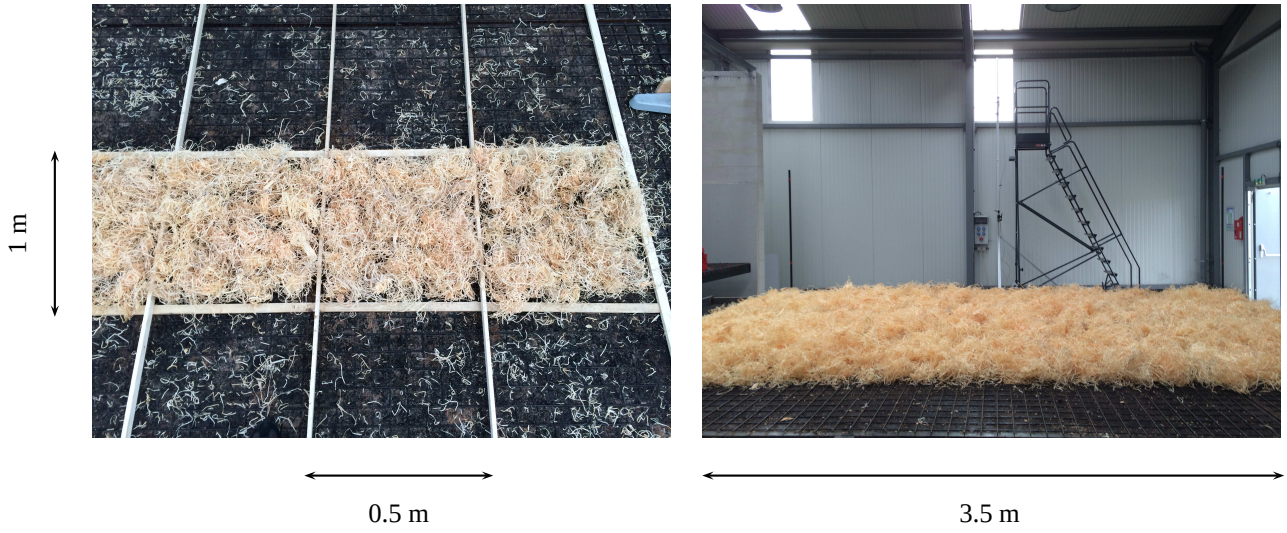

(a) Fuel bed preparation for 0.2 kg/m^2 (b) Fuel bed ready to test. Configuration with a 3.5 m width for 1 kg/m^2

Figure 5 Examples of different wood wool beds

- Net Heating Value (NHV) in the basis of wet mass: 16 480 kJ/kg;
- Low Heating Value (LHV) in the basis of oven dry mass: 18 290 kJ/kg;
- Higher Heating Value (HHV) in the basis of oven dry mass: 19 560 kJ/kg;
- Heat capacity of the dry matter (Cp_{dry}): 1 430 J/kg/K.

2.2 Vegetation bed

For each experiment, the vegetation is put on a combustion table, made of steel without insulated material on the top surface. This combustion table can be inclined from -25° to 25° (not used in this contribution) to study the slope effect on the fire propagation.

Vegetation load ρ [kg/m^2]	0.1	0.2	0.3	0.4	0.5	0.6	0.7	0.8	0.9	1
Mean vegetation bed height [cm]	1.6	3.5	4.4	5.7	8.7	7.8	10.2	12.3	12.2	14.25
Mean bulk density [kg/m^3]	7.1	6.4	7.0	7.4	5.9	7.7	6.9	6.6	7.4	7.0

Table 4 Values of the mean bed height function of the vegetation load

Heat transfer on fire front can be affected by the presence of some insulated materials beneath the fuel bed. Marchand [28] conducted some supplementary experiments using 10 cm-width cellular concrete as insulated materials. For these tests, the vegetation loads are set at 0.5 kg/m^2 and the fuel bed dimensions are 2 m x 2 m. The results showed that the Rate Of Spread (ROS) was not affected (relative discrepancies lower than 5%). On the contrary, the flame zone depth is influenced by the presence of cellular concrete beneath the vegetation. The value of e_f decreases about 25% (from about 35 cm with insulated bench to 26 cm without insulated material).

Figures 5(a) and 5(b) show examples of vegetation beds. The height of this kind of vegetation bed depends on the porosity of the vegetation. Table 4 gathers the mean vegetation bed heights for several vegetation loads, from 0.1 kg/m^2 to 1 kg/m^2. These mean data were collected over 85 vegetation beds. The vegetation bed heights are in the range of 1.6 cm to 14.25 cm.

Figure 6(a) presents the evolution of the mean vegetation bed height as function of vegetation load. This figure shows a quasi-linear increase of the mean vegetation bed height with the vegetation load. The discrepancy observed on vegetation bed height for a given vegetation load mainly depends on the person in charge of fuel bed preparation.

For the results presented in Figure 6(a) and others in the following, the error bars correspond to the 95% confidence intervals (CI). For these calculations for the feature X, its mean value ($\bar{X}$) and its mean standard deviation (σ) are estimated. We make the simple assumption that experimental data on X is known to be normally distributed and that the standard deviation σ is known. Confidence intervals are in the range of $\left(\bar{X} - 1.96\frac{\sigma}{\sqrt{n}},\ \bar{X} + 1.96\frac{\sigma}{\sqrt{n}}\right)$, where n is the sample size.

Vegetation bulk density is a function of vegetation load and height of the fuel bed. Table 4 gives the bulk density estimated for each vegetation load based on the mean vegetation bed height. The bulk density is given as a function of vegetation

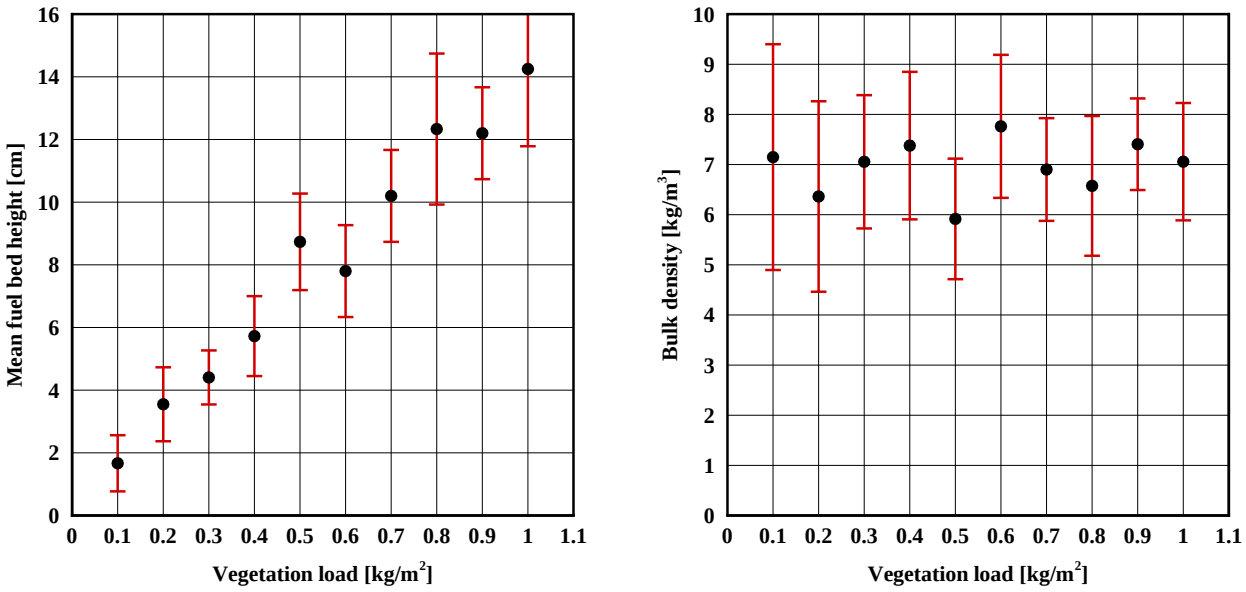

(a) Mean fuel bed height function of fuel bed load (b) Corresponding bulk density function of fuel bed load

Figure 6 Vegetation bed features regarding the vegetation load evolution

load (Figure 6(b)). These values vary between 5.6 kg/m^3 and 7.3 kg/m^3 and are very sensitive to fuel bed heights. Also calculation of the bulk density considered moisture content of vegetation and differs of the dry bulk density usually used. A mean value for bulk density can be estimated at 6.94 kg/m^3 with a mean standard deviation of 0.7 kg/m^3. The corresponding porosity is evaluated at 98.72%. The packing ratio β is the ratio of fuel volume to fuel bed volume. It is estimated at 0.0128. This value is in agreement with the one obtained by Dickinson *et al.* [20] which is about 0.014 for Excelsior.

For each experiment, vegetation was distributed using the same experimental method: the vegetation bed surface was divided into small areas (about 0.25 m^2, as it can be seen in Figure 5(a)) with the same fuel load. The method ensured a quasi-homogeneous spatial distribution of fuel. Figure 5(b) gives an example with a vegetation load of 0.5 kg/m^2. The mean bed height is estimated at 8.5 cm.

Figure 7 Example of a fire spread test on a burning table - Fuel bed dimensions set at 2 m x 2 m for a vegetation load estimated at 0.5 kg/m^2

2.3 Ignition

Two operators simultaneously ignite the extremities of the fuel bed width using welding torches. This process allows a quite instantaneous ignition. For largest beds, a small line of alcohol helps the vegetation ignition. An example of a fire spread is shown in Figure 7 for a 2 m $\times$ 2 m vegetation area with a 0.5 kg/m^2 fuel load. For this configuration, the experimental test lasts approximately 130 s and the steady state was reaching 30 seconds after the ignition, corresponding to a reached total distance of 50 centimeters.

2.4 Surrounding conditions

The ambient conditions, included temperature and relative air humidity, were recorded before each test with a local indoor weather station. Figures 8(a) and 8(b) give the distributions of air temperature and air relative humidities respectively for the 85 experiments considered in this study. These distributions show a large dispersion of these two meteorological features depending on climatic conditions (experiments were carried out during spring, summer and fall).

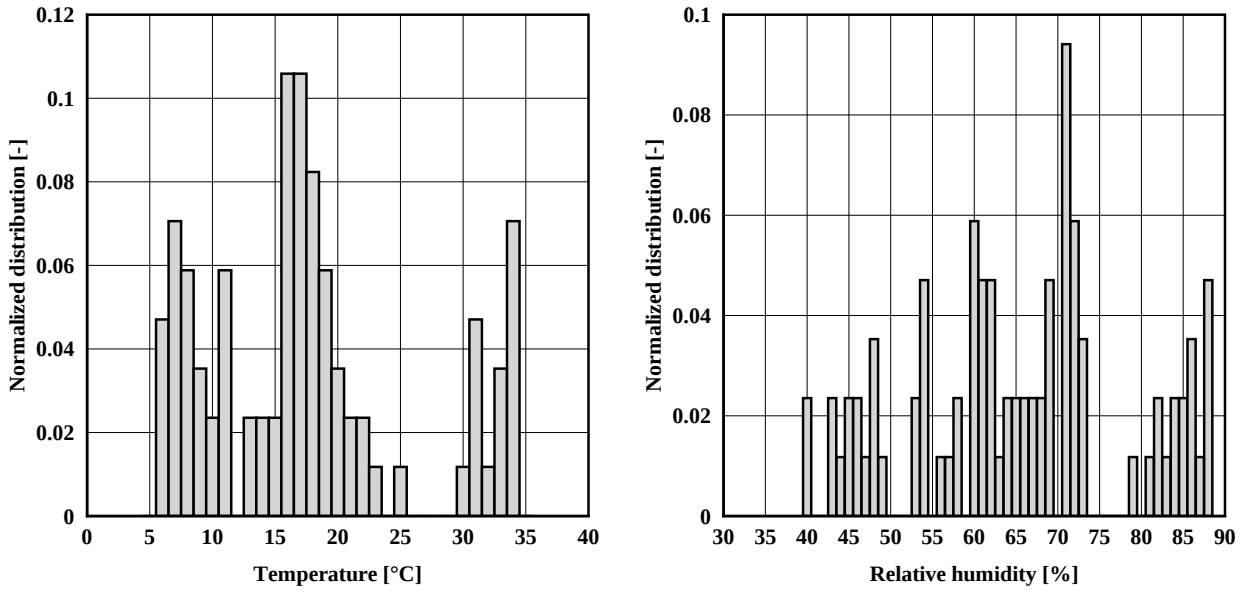

(a) Distribution of ambient air temperature (b) Distribution of ambient air relative humidity

Figure 8 Surrounding conditions measured during the experimental campaign

2.5 Fire front reconstruction

2.5.1 Acquisition

Two monochrome cameras (Le165MP by LUMENERA) filmed the fire spread from a height of 2.50 m above the ground:

- camera #1 tracked the ignition fire front;
- camera #2 tracked the extinction fire front.

Results are 8 bits grayscale images with a resolution of 1376 $\times$ 1032 pixels. Monochrome camera sensors ensure better sensitivity and details than color cameras. The acquisition frequency is 1 Hz considering a rate of spread around 1 to 2 cm/s for this kind of fires. The image acquisition system was started before each fire ignition but only images acquired after the ignition phase were considered.

2.5.2 Fire front detection

An image segmentation processing method developed with MATLAB Image Processing Toolbox detects the fire fronts from the grayscales images. These fronts were extracted by a six steps image processing algorithm, as illustrated in Figure 9:

(i) loading of the grayscale image and elimination of noise outside the region of interest drawn by the experimentalist;
(ii) use of the multi-levels segmentation of Otsu algorithm [22] after determination of a maximum number of levels based on the brightness of the fuel bed;
(iii) segmentation with the maximal level detected by Otsu algorithm;
(iv) construction of a mask image by applying a convex hull algorithm on the binary image;
(v) application of an active contour algorithm [23] using the segmented image and mask to limit the detection of hulls inside fire and to smooth the fire front;
(vi) straight lines scanning along Z direction to detect the first pixels equal to 1 (fire zone).

2.5.3 Fire front reconstruction

Results of the image processing are pixels points that represent ignition or extinction front. The objective is to correct the perspective effects: a Direct Linear Transformation algorithm (DLT) converts pixel coordinates from image plane to real physical plane (in meters). This method is well described by Pastor *et al.* [24]. This algorithm required a calibration step, consisting in identification of four referential points. The vertical position of spots is 8.5 cm which corresponds to the height of fuel bed for fuel loads larger than or equal to 0.5 kg/m^2. For lower fuel loads, surface spots were directly set on the fuel and the height of each corner was recorded [28].

We applied the DLT algorithm for the entire duration of fire propagation to reconstruct ignition and extinction fronts. Figure 10 shows an example of a fire front tracked in a binary image which is projected to the real space to determine its real geometry. The black dots are reference points used by the DLT algorithm.

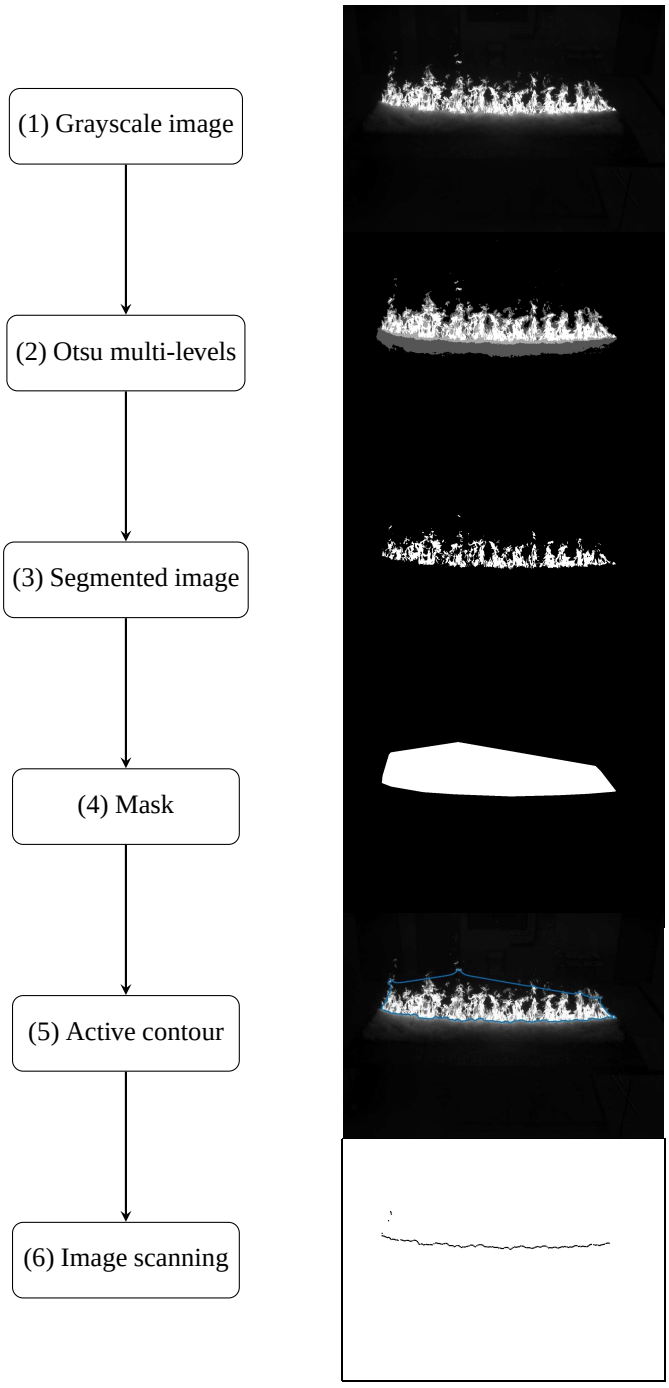

Figure 9 Image processing for fire front reconstruction: case of the ignition front

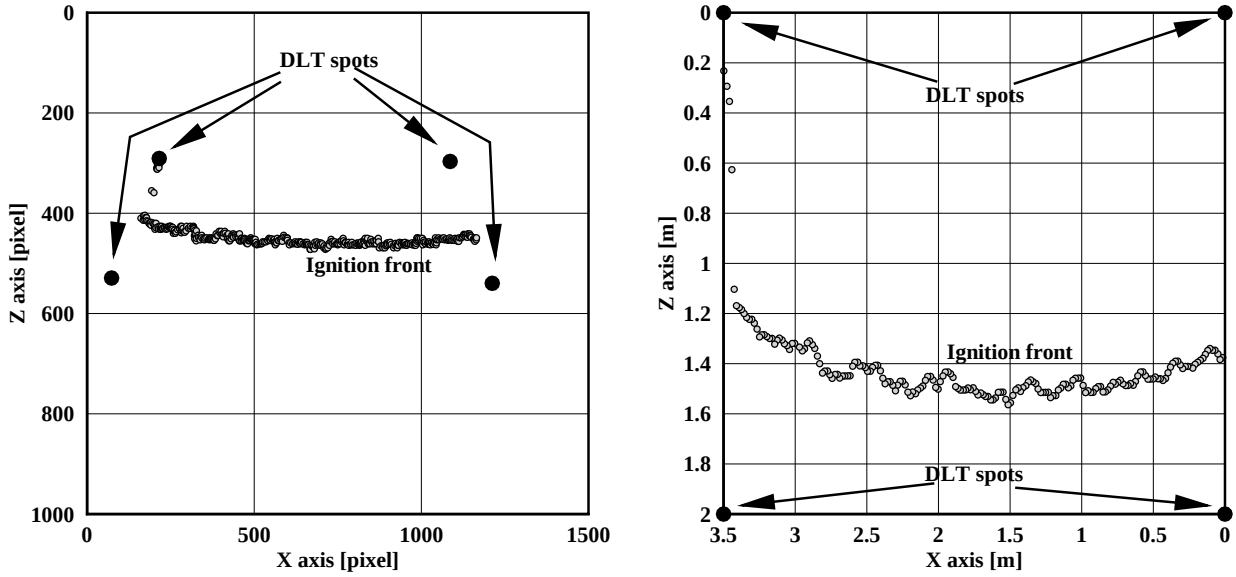

(a) Image plane (b) Physical plane

Figure 10 Examples of DLT algorithm applied on the ignition front for an experiment with a 3.5 m-fuel bed width

3. PROMETHEI DATABASE

3.1 Database presentation

All data from the 85 fire spread experiments are available on the laboratory website [19]. It includes fire front positions as a function of time. Users can download these data as a Matlab file with a name including the experiment number. For each file, user will find a header describing characteristics of the fire spread experiment (fuel load, air relative humidity, moisture content, air temperature, fuel bed width, and length). Two matrices describe ignition and extinction fire front positions. On a given line of a matrix, the first column gives X position, the second one, Z position and the third one indicates the corresponding time.

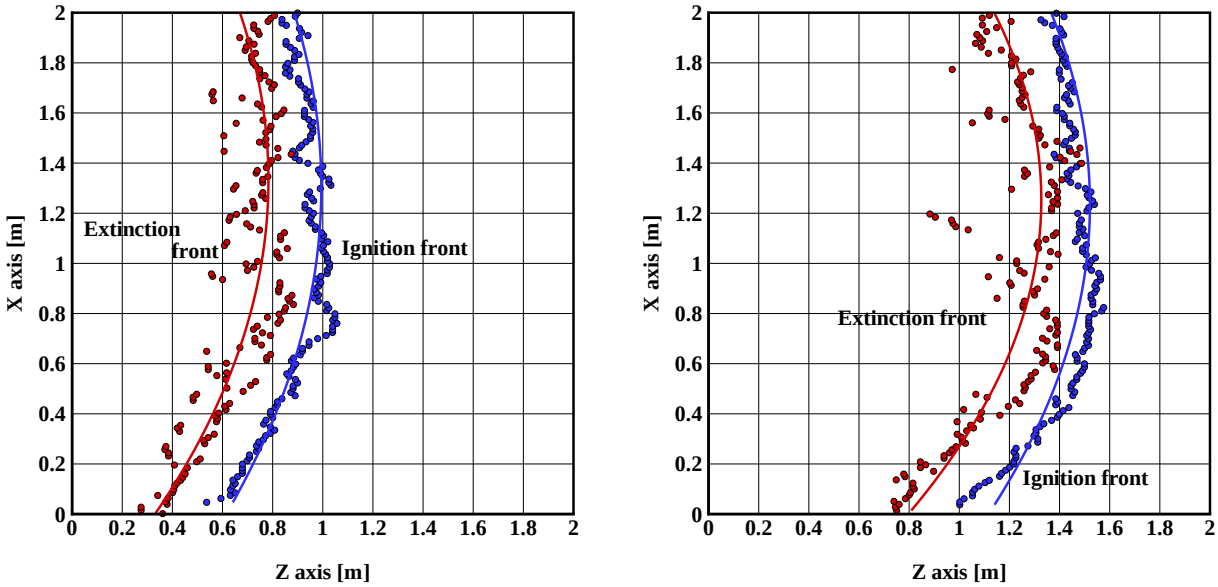

(a) Ignition front at Z = 1 m

(b) Ignition front at Z = 1.5 m

Figure 11 Ignition and extinction fronts reconstruction for a vegetation load set at 0.5 kg/m^2 and a fuel length set at 2 m

3.2 Analysis of the experiments

In this subsection, we give a simple description of methods used to post-process all images obtained from wood burning experiments. We chose to describe the geometry of ignition and extinction fronts as a second order polynomial equation:

$$Z^{\text{front}} = aX^2 + bX + c \tag{4}$$

where X corresponds to one hundred equally distributed positions between 0 and the maximum bed width. A least-square method estimates the coefficients a, b, and c. We adopted the middle position of fuel bed width to describe position of fire fronts Z over time. We assume this position to be close to the most advanced position. The mean relative discrepancies between the real fire front position and its polynomial representation can achieve 30% once the steady state is reached. Then the ROS is evaluated with a linear regression of the middle position of the ignition fire fronts as a function of time. The flame zone depth is the average distance between extinction and ignition front positions.

Figure 11(a) and 11(b) show two examples of a reconstruction of ignition and extinction fronts respectively at two different positions (1 m and 1.5 m) for a fuel bed width of 2 m. The time gap between these two images is estimated about 36

seconds. In these conditions, the ignition front travels about 53 cm (for the center line at X = 1 m), giving a Rate Of Spread (ROS) of 1.5 cm/s.

We note that second order polynomial function describes well the shape of the ignition front, as it is depicted in Figure 11. Based on the polynomial representations, the flame zone depth (e_f) varies from 21 cm to 20 cm, respectively, in Figure 11(a) and 11(b).

However, extinction fire front reconstruction is affected by the presence of smouldering particles that were not eliminated by the image processing, and affects the thickness of the flaming fire front measurement. The polynomial function still provides the mean curvature of the extinction fire front. In both cases, we observe an evolution of fire front morphology over time. The fire front bent during propagation until reaching a steady state.

The fire front length (l_f) is estimated as the integral along the ignition front:

$$l_f = \int_C \mathrm{d}s \tag{5}$$

where C is the contour of the ignition front and s the curvilinear coordinate. In considering the parametric representation of the contour (C) based on Eq.(4) (polynominal representation), the fire front length is obtained by analytical integration of Eq.(5):

$$l_f = \frac{1}{a}\left(\arcsin\left(2aL_w + b\right) - \arcsin\left(b\right) + \left(aL_w + b\right)\sqrt{\left(aL_w + b\right)^2 + 1} - b\sqrt{\left(b^2 + 1\right)}\right) \tag{6}$$

The analyze of the results provided by the database has proved that the ignition front length (l_f) reaches a value close to the fuel bed width (L_w), especially when the fuel bed load is larger than 0.2 kg/m^2. The maximal relative discrepancies between l_f and L_w are about 4%, demonstrating that the ignition front curvature is not strong.

The study is dedicated to analyze fire propagation dynamics (through the Rate Of Spread ROS or the flame zone depth e_f) regarding to fuel bed parameters. Supplementary data on the flame geometry can be found in Marchand [28].

4. SUMMARY OF MAIN RESULTS

All the results presented above, are extracted from the PROMETHEI database and analyze the single effects of fuel bed

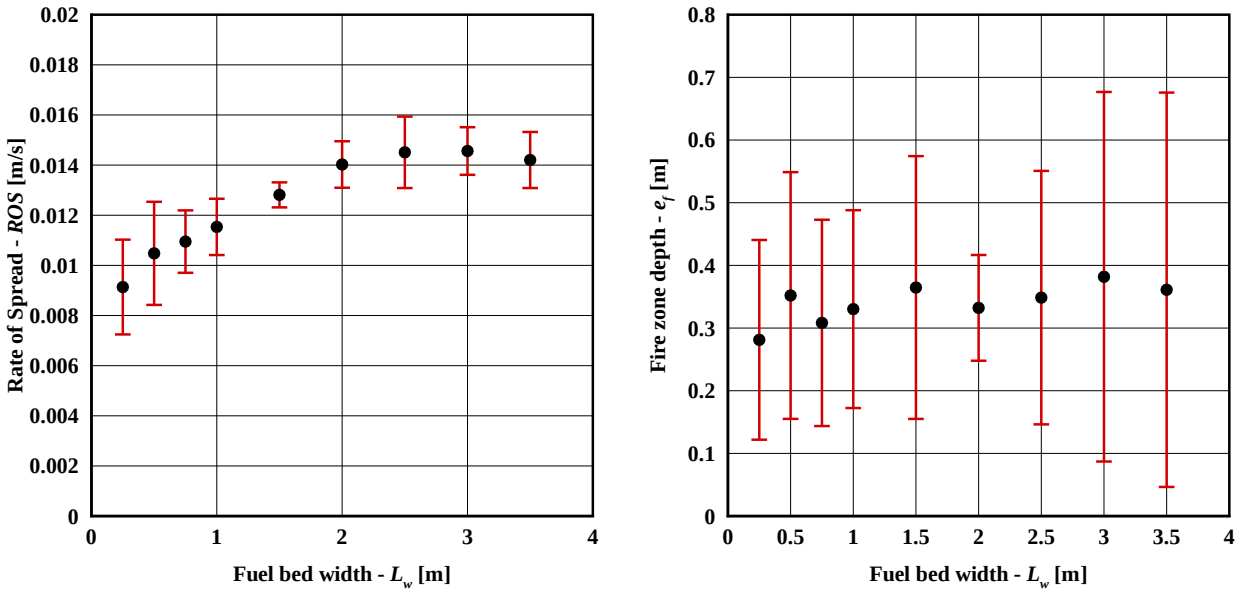

(a) Rate Of Spread (ROS) evolution as function of fuel bed width

(b) Flame zone depth evolution as function of fuel bed width

Figure 12 Effect of fuel bed width on the fire front features

width and fuel bed load on the fire propagation. For the following discussions, only the steady state of the fire spread is concerned.

Moreover, the results presented in this section can be affected by the environmental conditions. The effects of ambient temperature or/and relative humidity are taking into account in the error bars plotted in the figures below.

4.1 Effect of fuel bed width

Results of 45 experiments with a fuel load of 0.5 kg/m^2 for 9 different fuel bed widths are presented from 0.25 to 3.5 m: each experiment is repeated 5 times. Figure 12(a) presents the ROS as a function of fuel bed width L_w. A good reproducibility is observed between experiments with the same width. The uncertainty is more important for small widths due to the limited spatial resolution, the low luminosity of fire and the effect of the disperse medium (ignition front geometry strongly depends on spatial distribution of wood wool). The biggest discrepancy is about 0.003 m/s for the 0.5 m-fuel bed width. The ROS increases at low values of fuel bed width and seems to reach a constant value of about 1.5 cm/s for a 2 m fuel bed width and beyond. This trend was already observed by Naville [25] for experimental fire propagations

on beds composed of Excelsor. Similar experiments without slope performed by Adam *et al.* [26] demonstrated that this asymptotic ROS reaches 1.7 cm/s for a fuel bed load set at 0.5 kg/m^2 (and thus a 8.7 cm-fuel bed height according to Table 4).

As presented in Figure 12(a), the Rate Of Spread (ROS) seems to follow a power law function of the fuel bed width (L_w). An attempt has been done on the previous data to identify the coefficients of the power law by a least-square method. The results is given by:

$$ROS = 0.0118\ L_w^{0.19} \tag{7}$$

This analytical form of ROS provides a maximal relative discrepancy between the experimental data and the predicted values given by Eq.7, reaching 15% and the mean relative discrepancy is about 4%, proving the efficiency of the previous correlation.

The flame zone depth e_f is presented in Figure 12(b) as a function of fuel bed width L_w. The mean results vary between 0.28 m and 0.38 m. Discrepancies are more significant than those obtained for ROS. Smouldering particles affect the reconstruction of extinction front and may lead to fluctuations in the flame zone depth estimation. A change in ambient conditions may also partly explain the discrepancy since tests were carried out in various seasons.

On the basis of the previous flame zone features, the fire front intensities can be evaluated for all the experiments using the Byram's fire intensity relationship [27] for steady fires:

$$I_{\text{Byram}} = ROS\ \rho\ LHV \tag{8}$$

where ρ stands for the fuel load. For each experiment, the intensities vary from 70 to 120 kW/m. The values seem to reach a constant intensity close to 120 kW/m for a 2 m-fuel bed width and beyond, as Rate Of Spread is constant.

Generally, in fire applications, it is more convenient to use the heat provided by the flame zone using the Heat Release Rate (HRR) than fire front intensities. This feature is calculated, in steady state by multiplying the intensity by the flame zone length:

$$HRR = I_{\text{Byram}}\ l_f \tag{9}$$

As it is previously demonstrated, the fire front length (l_f) is close to fuel bed width (L_w). For a quasi-constant fire intensity

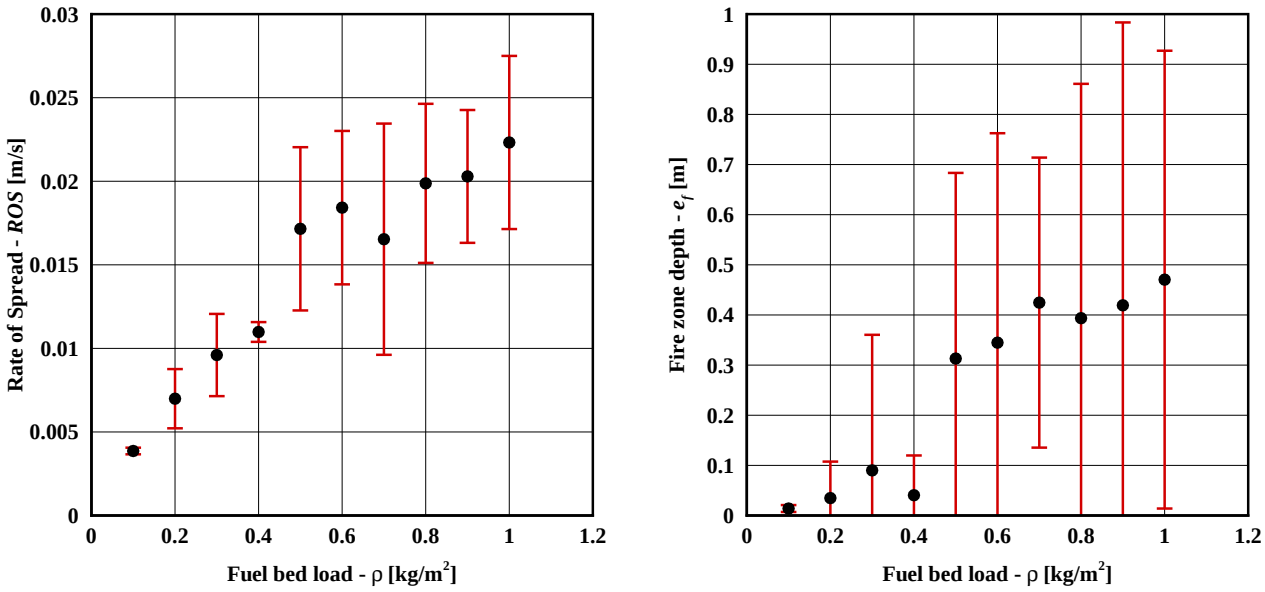

(a) Rate Of Spread (ROS) evolution as function of fuel bed load (b) Flame zone depth evolution as function of fuel bed load

Figure 13 Effect of fuel load on the fire front features

of 120 kW/m, the maximal Heat Release Rate obtained during this experimental campaign can reach 420 kW.

4.2 Effect of fuel load on fire spread

Results of 40 experiments involving 10 different vegetation loads between 0.1 and 1 kg/m^2 with a fuel bed width of 2 m. The geometry of the fire front for the lowest fuel loads (0.1 and 0.2 kg/m^2) are modelled as the average positions of the ignition and extinction. ROS was estimated at the middle position of the ignition fire front. Figure 13(a) presents ROS evolution as a function of vegetation load. The ROS globally increases with fuel load from 0.3 cm/s for the lowest load to 2.6 cm/s in average for the highest load. Reproducibility tests showed discrepancy up to $\pm$ 0.5 cm/s as compared to the average values. Such a discrepancy is significant but can be explained by ambient conditions (experiments carried out at different seasons) and vegetation height variations.

These results are in good agreement with the ones performed by Morandini *et al.* [29] where Excelsior is used to compose the fuel beds. With no inclinaison, Rate of Spread (ROS) varies from 1.1 cm/s for 0.2 kg/m^2 up to 1.95 cm/s for 0.6 kg/m^2, that matches the results provided by the present study.

Figure 13(b) gives flame zone depth evolution e_f as a function of vegetation load. As it can be noted, the flame zone depth (e_f) increases with the fuel bed load and varies from 1.4 to 47 cm. The uncertainty on the flame zone depth rises with fuel load probably due to the presence of smouldering particles in important numbers after the fire front spread.

Based on these experiments, the Byram's intensity estimation shows that the values can vary from 6.3 kW/m up to 360 kW/m and Heat Release Rate (HRR) can reach 720 kW for the maximal fuel bed load considered in the present study.

5. CONCLUSION

This study presents 85 experiments on vegetation fire spread at laboratory-scale with wood wool on burning table. An image processing method extracts ignition and extinction fronts based on grayscale images acquired during propagation tests. An online, free-accessed database gathers all fire front positions for all experiments. This database aims at validating and calibrating fire spread models at laboratory-scale. In future work, this database will be extended with experiments including slope and wind effects involving more data from other sensors like heat flux gauges, thermocouples and Particle Image Velocimetry in particular. Also, one of remaining objective is to move from small fire spread experiments to larger fire spread experiments in order to study up-scaling effects.

6. ACKNOWLEDGMENT

The authors would like to thank Juan Pablo Chica Cano, Nicolas Trevisan, Pascal Laboureur, Alexandre Braconnier, Rabah Mehaddi, Thomas Gasparotto, Jonathan Gérardin and Alexandre Jenft for their valuable help when conducting tests. Yann Rogaume from the LERMAB laboratory and Thomas Rogaume from the PPRIME laboratory are also acknowledged for providing characteristic properties for wood wool.

APPENDICES

Probability density functions

Weibull law The probability density function of a Weibull law is given by,

$$f(x) = \frac{b}{a}\left(\frac{x}{a}\right)^{b-1} \exp\left(-\left(\frac{x}{a}\right)^{b}\right) \tag{10}$$

where b is the shape parameter and a is the scale parameter of the distribution.

Normal law The probability density function of a normal or Gaussian distribution is given by,

$$f(x) = \frac{1}{\sqrt{2\pi}\sigma} \exp\left(-\frac{1}{2}\left(\frac{x-\mu}{\sigma}\right)^{2}\right) \tag{11}$$

where μ is the mean of the distribution and σ the standard deviation.

REFERENCES

[1] A.L. Sullivan. Wildland surface fire spread modelling, 1990–2007. 1: Physical and quasi-physical models. *International Journal of Wildland Fire*, 18(4):349–368, 2009.

[2] A.L. Sullivan. Wildland surface fire spread modelling, 1990–2007. 2: Empirical and quasi-empirical models. *International Journal of Wildland Fire*, 18(4):369–386, 2009.

[3] A.L. Sullivan. Wildland surface fire spread modelling, 1990–2007. 3: Simulation and mathematical analogue models. *International Journal of Wildland Fire*, 18(4):387–403, 2009.

[4] R.C. Rothermel. A mathematical model for predicting fire spread in wildland fuels. *USDA Forest Service*, 1972.

[5] W. Mell, M.A. Jenkins, J. Gould, and P. Cheney. A physics-based approach to modeling grassland fires. *International Journal of Wildland Fire*, 16(1):1–22, 2007.

[6] R.R. Linn and P. Cunningham. fires using a coupled atmosphere–fire model: basic fire behavior and dependence on wind speed. *Journal of Geophysical Research: Atmospheres*,110(D13), 2005.

[7] D. Morvan, S. Méradji, and G. Accary. Physical modelling of fire spread in grasslands. *Fire Safety Journal*, 44(1):50–61, 2009.

[8] A. Collin, D. Bernardin, and O. Séro-Guillaume. A physical-based cellular automaton model for forest-fire propagation. *Combustion Science and Technology*, 183(4):347–369, 2011.

[9] B. Porterie, N. Zekri, J.P. Clerc, and J.C. Loraud. Modeling forest fire spread and spotting process with small world networks. *Combustion and Flame*, 149(1):63–78, 2007.

[10] M.C. Rochoux, B. Cuenot, S. Ricci, A. Trouvé, B. Delmotte, S. Massart, R. Paoli, and R. Paugam. Data assimilation applied to combustion. *Comptes Rendus Mécanique*, 341(1):266–276, 2013.

[11] N.P. Cheney, J.S. Gould, and W.R. Catchpole. The influence of fuel, weather and fire shape variables on fire-spread in grasslands. *International Journal of Wildland Fire*, 3(1):31–44, 1993.

[12] N.P. Cheney and J.S. Gould. Fire growth in grassland fuels. *International Journal of Wildland Fire*, 5(4):237–247, 1995.

[13] P.A.M. Fernandes. Fire spread prediction in shrub fuels in Portugal. *Forest ecology and management*, 144(1):67–74, 2001.

[14] D. Morvan, G. Accary, S. Meradji, N. Frangieh and O. Bessonov. A 3D physical model to study the behavior of vegetation fires at laboratory scale. Fire Safety Journal, 101, 39-52. *Fire Safety Journal*, 101:39–52, 2018.

[15] R.C. Rothermel and H.E. Anderson. Fire spread characteristics determined in the laboratory. *U.S. Forest Service*, 1966.

[16] W.R. Catchpole, E.A. Catchpole, B.W. Butler, R.C. Rothermel, G.A. Morris, and D.J. Latham. Rate of spread of free-burning fires in woody fuels in a wind tunnel. *Combustion Science and Technology*, 131(1-6):1–37, 1998.

[17] J. B. Fang and F. R. Steward (1969). Flame spread through randomly packed fuel particles. *Combustion and flame*, 13(4), 392–398, 1969.

[18] D. R. Weise, X. Zhou, S. Mahalingam and J. Chong, Marginal fire spread in live fuel beds–horizontal fuels *USDA Forest Service Research Data Archives*, 2015.

[19] A. Marchand, S. Ferriere, A. Collin, P. Boulet, Z. Acem, F. Demeurie, and J.Y. Morel. *PROMETHEI database*, 2017 (accessed November 30, 2018). `https://lemta.univ-lorraine.fr/promethei_database.html`.

[20] M.B. Dickinson, E.A. Johnson, and R. Artiaga. Fire spread probabilities for experimental beds composed of mixedwood boreal forest fuels. *Can. J. For. Res.*, 43:321–330, 2013.

[21] C. Di Blasi. Modeling chemical and physical processes of wood and biomass pyrolysis. *Progress in Energy and Combustion Science*, 34:47–90, 2008.

[22] N. Otsu. A threshold selection method from gray-level histograms. *Automatica*, 11(285-296):23–27, 1975.

[23] T.F. Chan and L.A. Vese. Active contours without edges. *Image processing, IEEE transactions on*, 10(2):266–277, 2001.

[24] E. Pastor, A. Àgueda, J. Andrade-Cetto, M. Muñoz, Y. Pérez, and E. Planas. Computing the rate of spread of linear flame fronts by thermal image processing. *Fire Safety Journal*, 41(8):569–579, 2006.

[25] L. Naville Experimental and numerical study of flame propagation on porous fuel : applications to forest fire PhD thesis. Aix-Marseille II University, 1997.

[26] B.A. Adam, N.K. Akafuah, M. Finney, J. Forthofer, and K. Saito. A study of flame spread in engineered cardboard fuelbeds. Part II: Scaling law approach. In *Seventh International Symposium on Scale Modeling, ISSM-7, Hirosaki, Japan*, 2013.

[27] G.M. Byram. Combustion of forest fuels. *Forest fire: Control and use*, 1:61–89, 1959.

[28] A. Marchand Wildland fire propagation: lab-scale experimentations and validation of a numerical simulator. PhD thesis. Lorraine University, 2016.

[29] F. Morandini, X. Silvani, J.L. Dupuy, and A. Susset Fire spread across a sloping fuel bed: Flame dynamics and heat transfers *Combustion and Flame*, 190:158-170,2018.